

## Article

# Experimental and Theoretical Study for a Displacement-Controlled Design Method of Embedded Cantilever Retaining Walls (Piles)

Xiaozhen Fan <sup>1,2,3</sup> , Changjie Xu <sup>4,5,\*</sup> and Luju Liang <sup>1,2,3</sup>

<sup>1</sup> College of Engineering, Hangzhou City University, Hangzhou 310015, China; fanxz@hzcu.edu.cn (X.F.); lianglj@hzcu.edu.cn (L.L.)

<sup>2</sup> Key Laboratory of Safe Construction and Intelligent Maintenance for Urban Shield Tunnels of Zhejiang Province, Hangzhou 310015, China

<sup>3</sup> Zhejiang Engineering Research Center of Intelligent Urban Infrastructure, Hangzhou 310015, China

<sup>4</sup> School of Civil Engineering and Architecture, East China Jiaotong University, Nanchang 330013, China

<sup>5</sup> Research Centre of Coastal and Urban Geotechnical Engineering, Zhejiang University, Hangzhou 310015, China

\* Correspondence: xucj@zju.edu.cn

**Abstract:** Displacement control is critical to the design of retaining walls, especially in urban areas, to avoid any potential damage to adjacent structures during excavations. In this study, model tests are first conducted to investigate the stress and deformation mechanisms of an embedded cantilevered retaining (ECR) wall during excavations. The development of the wall top displacement and the active and passive earth pressures acting on the ECR walls during excavations are studied. Upon the experimental observations, a displacement-dependent earth pressure coefficient is proposed to derive an analytical solution to predict both the active and passive earth pressure acting on the ECR wall (pile), where the displacement value and displacement mode of the ECR wall (pile) are taken into account. Comparisons between the model predictions and test results are carried out. A good agreement is observed, which shows the validity of the proposed solution. Based on the proposed solution, a displacement-controlled method for the design of ECR walls (piles) that takes into account the location of the rotation point is proposed. Parametric studies are conducted to demonstrate the impact of deformation control and excavation depth on the design parameters of ECR walls (piles).

**Keywords:** excavation; embedded cantilever retaining wall; design method; displacement control; earth pressure



**Citation:** Fan, X.; Xu, C.; Liang, L. Experimental and Theoretical Study for a Displacement-Controlled Design Method of Embedded Cantilever Retaining Walls (Piles). *Sustainability* **2023**, *15*, 9831. <https://doi.org/10.3390/su15129831>

Academic Editor: Claudia Casapulla

Received: 5 May 2023

Revised: 6 June 2023

Accepted: 18 June 2023

Published: 20 June 2023



**Copyright:** © 2023 by the authors. Licensee MDPI, Basel, Switzerland. This article is an open access article distributed under the terms and conditions of the Creative Commons Attribution (CC BY) license (<https://creativecommons.org/licenses/by/4.0/>).

## 1. Introduction

Embedded cantilever retaining (ECR) walls (piles) are commonly adopted in excavations when the excavation depth is generally less than 5 m [1]. However, it is widely recognized that the ground movements induced by excavations can affect adjacent structures [2–16]. Therefore, in order to avoid any potential damage to the adjacent properties and improve the sustainability of the neighboring environment, the concept of performance-based design has been adopted since the 1990s, which emphasizes the importance of deformation control in the design of retaining walls [17–22].

To design the ECR walls based on deformation control, rational consideration of displacement-dependent earth pressure distribution is necessary. However, the existing analytical methods for the design of ECR walls are generally based on the limit equilibrium method [1,22–28]. Since the limit equilibrium analysis is valid only at the point of failure, which is hardly achieved in engineering practice, a safety factor is generally applied to keep the walls safe and serviceable under working conditions. The safety factor has been defined in different ways. For instance, the calculated embedment depth at failure is increased by an empirical factor  $F_d$  [23]; the soil strength parameters are reduced by a factor  $F_s$  [29,30]; or

the passive earth pressure on the dredged side is reduced by a factor  $F_p$  [23,29]. However, those safety factors heavily rely on empiricism and lack a theoretical basis.

Several researchers have made contributions to achieving an optimal design solution for ECR walls. Based on the mobilized strength design (MSD) method, Zhang et al. [19] proposed a critical evaluation for the model factor for cantilever deflection. Conte et al. [1] derived a simple-to-use solution for the earth pressure distribution of the ECR wall, taking into account the displacement pattern. Nandi and Choudhury [20] presented an analytical method for the displacement-controlled analysis of ECR walls in cohesion-less soils. However, a realistic and simple-to-use design method that can calculate the required embedment depth based on the deformation control is still to be explored.

In the present study, based on an assumed linear relationship between the earth pressure coefficient and soil displacement, this paper proposes a deformation-controlled design method for the calculation of the required embedment depth. Model tests are first conducted to investigate the deformation and earth pressure distribution of the ECR wall during excavations. Based on the experimental observations, a displacement-dependent earth pressure coefficient is proposed to derive an analytical solution to predict both the active and passive earth pressure acting on the ECR wall. The proposed solution is validated by comparing the proposed results with the existing and presented experiment results. On the basis of the proposed solution for earth pressure, a displacement-controlled method for calculating the embedment depth and the location of the rotation point of ECR is proposed. Parametric studies are conducted to demonstrate the impact of deformation control and excavation depth on the design parameters of retaining walls.

## 2. Model Test Scheme

### 2.1. The Designed Test Set Up

A soil tank with dimensions of 2600 mm × 600 mm × 1200 mm (length × width × height) was constructed to conduct the model tests, as shown in Figure 1.

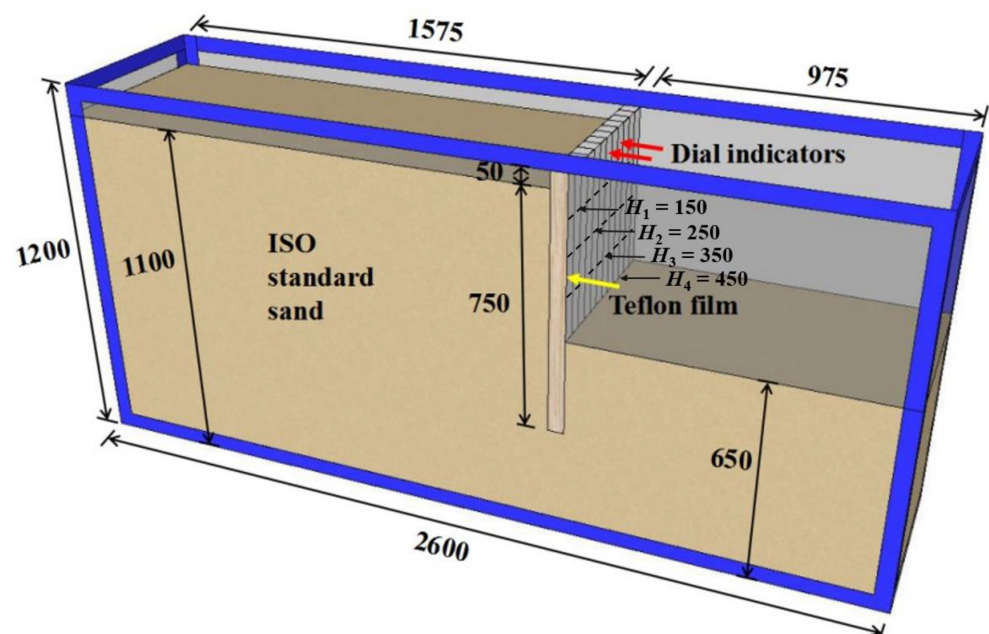


Figure 1. Schematic model test setup (unit: mm).

For each test, 12 contiguous rectangular polyvinyl chloride (PVC) tubes, with a cross section of 50 mm × 50 mm × 2.5 mm (length × width × wall thickness), were used to model the ECR wall. The length of the PVC tube is 800 mm, with 750 mm beneath the soil surface and 50 mm above the soil surface, for the convenience of arranging the dial

indicators (see Figure 1). Teflon (PTFE) film was attached to the side faces of the model piles to reduce any friction between the model piles and the sidewalls of the soil tank.

## 2.2. Backfilled Sand

The ISO Fujian standard sand (Figure 2a) with a specific gravity  $G_s$  of 2.65 is used as the backfilled material for all tests. As shown in Figure 2b,  $D_{60}$ ,  $D_{30}$ , and  $D_{10}$  of this dry sand are 0.96 mm, 0.69 mm, and 0.16 mm, respectively. In addition, the coefficients of uniformity and curvature are determined as 5.87 and 0.92, respectively. The sands are considered well-graded sands, according to ASTM D2487-11 [31].

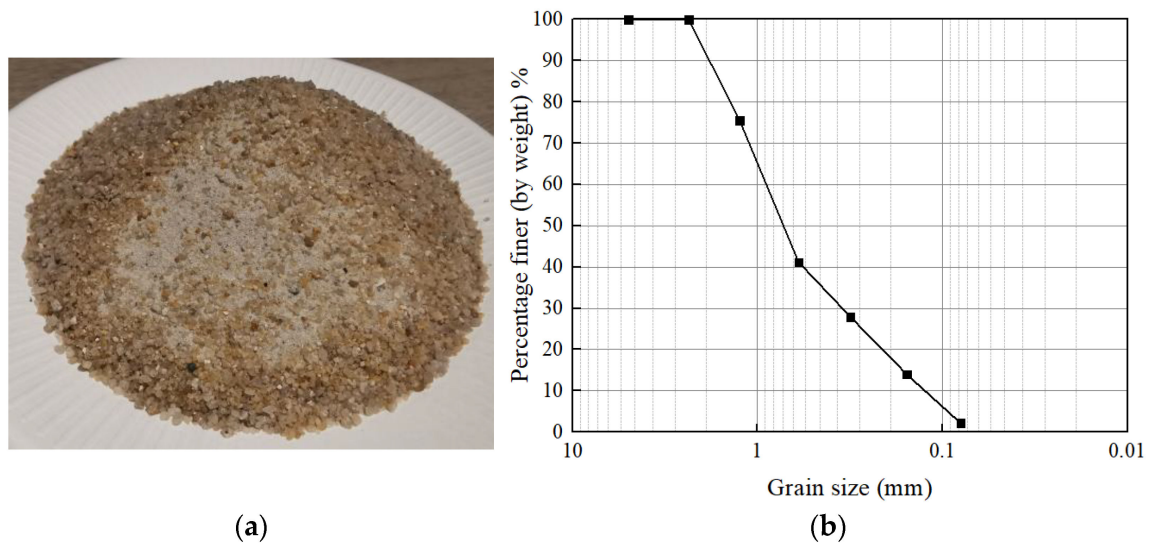


Figure 2. ISO Fujian standard sand: (a) Photo; (b) Grain size distribution.

To prepare the soil samples, sands are successively set into the soil tank with a sand raining device. The drop height of sand rain is maintained at 500 mm. Several small samples are prepared in a bucket following the same method. Then the dry unit weight  $\gamma$  and void ratio  $e$  of the test samples are measured as  $15 \text{ kN/m}^3$  and 0.73, respectively. The internal friction angle  $\phi$  of  $31.6^\circ$  is determined based on the direct shear test results of the samples, as shown in Figure 3a,b.

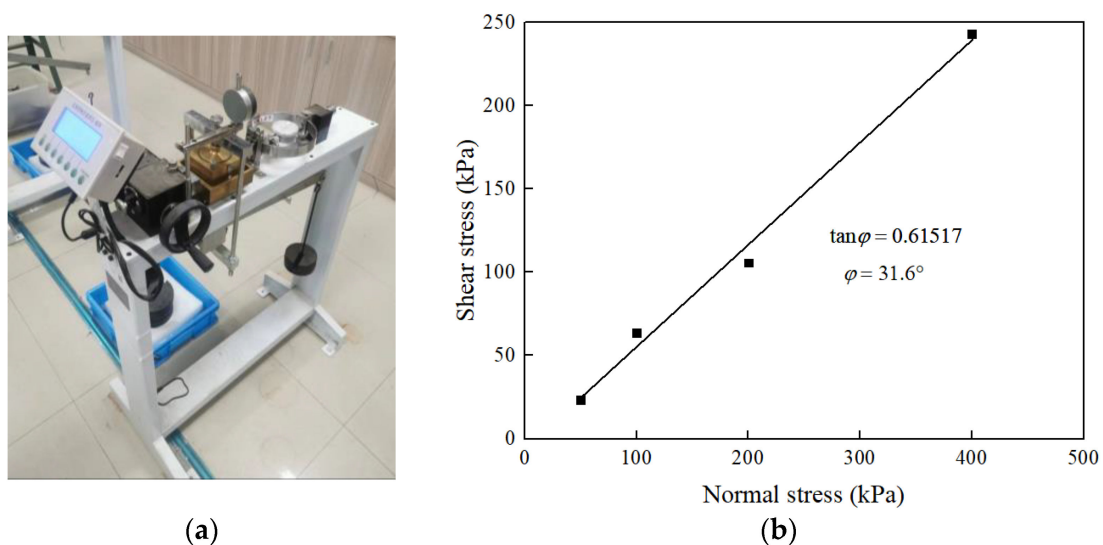


Figure 3. Direct shear test: (a) photo; (b) results of direct shear tests.

### 2.3. Similitude Relationship

The model piles used in this experiment can be regarded as lateral-loaded piles. As for lateral-loaded piles, according to the deflection differential equation of beams in material mechanics, the following equation can be obtained:

$$\frac{d^4s}{dz^4} + \frac{k_s b_0}{EI} s = 0, \quad (1)$$

in which  $s$  is the horizontal displacement of piles (m),  $z$  is the pile depth (m),  $k_s$  is the horizontal resistance coefficient ( $\text{N}/\text{m}^3$ ),  $b_0$  is the calculated width of pile (m),  $EI$  is the pile bending stiffness ( $\text{N}\cdot\text{m}^2$ ).

Therefore, the similarity of lateral-loaded piles should be satisfied as

$$\left(\frac{\lambda_s}{\lambda_L^4}\right) \frac{d^4s}{dz^4} + \left(\frac{\lambda_{k_s} \lambda_L^2}{\lambda_E \lambda_L^4}\right) \frac{k_s b_0}{EI} s = 0 \quad (2)$$

in which  $\lambda_L$  is the length scale,  $\lambda_{k_s}$  is the horizontal resistance coefficient scale, and  $\lambda_E$  is the elasticity modulus scale.

By simplifying, the similarity equation can be obtained as follows:

$$\frac{1}{\lambda_L} = \frac{\lambda_{k_s}}{\lambda_E} \quad (3)$$

Through theoretical and numerical results on lateral-loaded piles, Lin et al. [32] proved that the modulus of the pile is the major parameter controlling the similarity of deflection behavior between model piles and prototype piles. Therefore, it is suggested to select a model pile material with a modulus similarity ratio close to the geometry similarity ratio. In this paper, the geometry scaling ratio and modulus similarity ratio were set at 10. The parameters of the model pile are selected as follows:

(1) Selection of model pile width and length: take the width and length of the model pile as 50 mm, 0.75 m, respectively, which meet the geometry scale  $\lambda_D = \lambda_L = 1/10$ .

(2) Selection of model pile materials: The modulus of concrete and PVC is about  $3 \times 10^4$  MPa and  $3.5 \times 10^3$  MPa, respectively. Therefore, PVC is chosen as the material of the model piles, which approximately meets the modulus similarity  $\lambda_E \approx \lambda_L = 1/10$ .

The scale effect of the influence of soil particle size can hardly meet the strict geometric similarity in the 1 g model test. Fioravante [33] conducted centrifugal tests on bored piles of sand. It was verified that the scaling effect of soil particles could be ignored when the value of  $B/d_{50}$  was larger than a certain critical value, which was suggested to be between 40 and 50. Similarly, when the model test of a lateral-loaded pile is carried out, as long as the diameter  $B$  of the model pile can be guaranteed to be larger than a certain multiple of the characteristic particle diameter  $d_{50}$ , the scale effect of soil particle size can be neglected, and the model and prototype can be considered to meet the geometric similarity approximately. In this paper, the characteristic particle size  $d_{50}$  of the ISO standard sand was about 0.6 mm, and the diameter  $B$  of the model pile was 50 mm, meeting the above proportion. Therefore, the influence of the soil particle scale effect on the test results could be ignored.

### 2.4. Test Procedures and Measurements

The total excavation depth was 45 cm, and each excavation step was 10 cm, except for the first step, which is 15 cm, as shown in Figure 1.

The earth pressures acting on the piles were monitored by thirteen miniature earth pressure cells ( $\Phi 28 \text{ mm} \times 6.5 \text{ mm}$ ) installed on both the active and passive zone sides of PVC piles. The measuring range and the resolution of the earth pressure cells are 0–30 kPa and 0.01 kPa, respectively. Due to the small spacing between the earth pressure cells on the passive zone side, the passive earth pressure cells are placed separately on two

adjacent piles, as shown in Figure 4. The earth pressures were collected by a high-speed data acquisition system with a sampling frequency of 1 Hz.

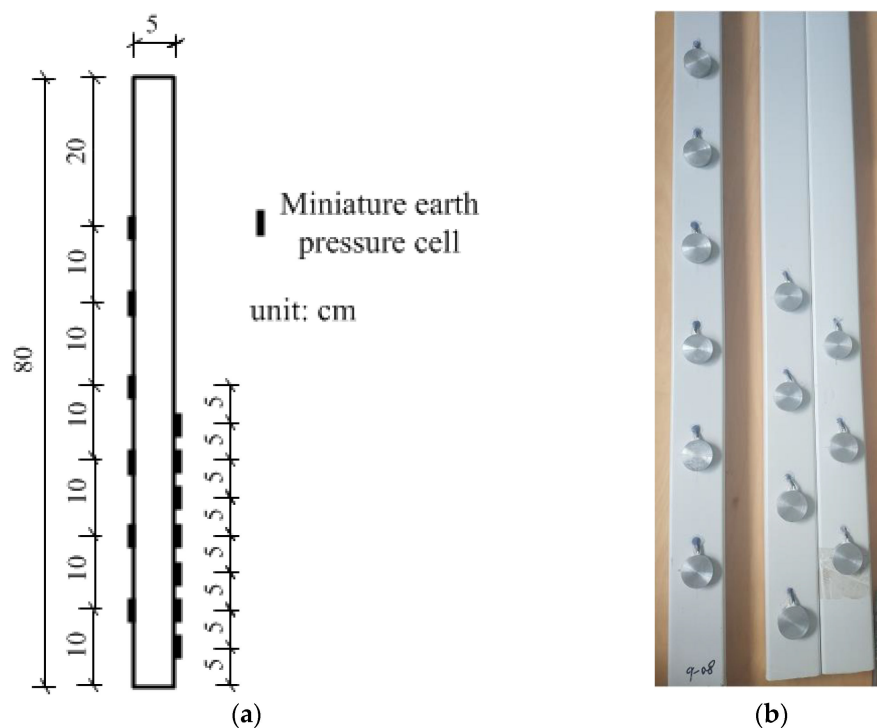


**Figure 4.** The placement of earth pressure cells: (a) schematic diagram; (b) photograph.

Horizontal displacements of the pile tops were measured using dial indicators with a measuring range of 5 cm and a resolution of 0.01 mm, as shown in Figure 5.



**Figure 5.** Physical diagram of the test model.

### 3. Test Results and Discussions

To easily understand the model test results and associate them with practical engineering, the results discussed in the following sections were all converted to prototype scale based on the scaling relationships stated above.

### 3.1. Displacement of Pile Top

As the excavation processed, the average horizontal displacements of the pile top increased with increasing excavation depths, reaching a maximum of 38.7 mm at an excavation depth of 4.5 m, as shown in Figure 6 and Table 1. In addition, it is found that with the increase in excavation depth, the displacement of pile tops increases at a faster rate, which indicates that more attention should be paid to the pile deformation in the excavation progress. For the reason that the ECR wall at the excavation depth of 4.5 m is subjected to a relatively large displacement, which may fall out of the non-limit earth pressure, only the analysis for excavation steps 1~3, which are in the range of the non-limit state, is carried out in the following section.

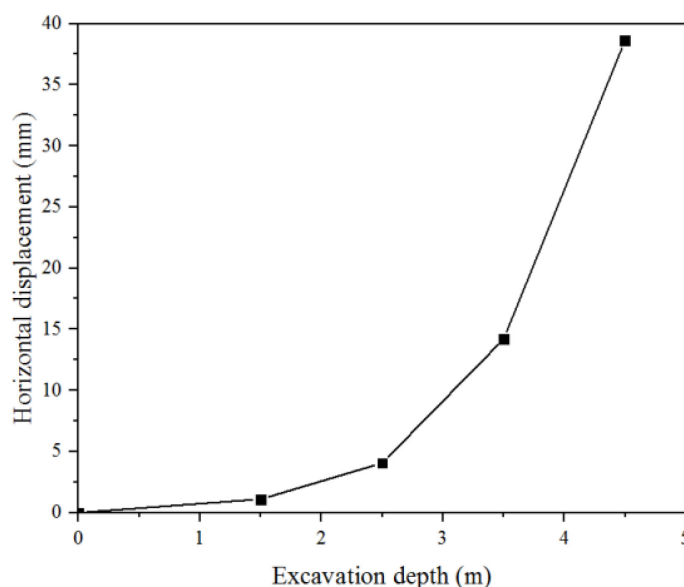


**Figure 6.** Average horizontal displacements of pile tops for different excavation depths.

**Table 1.** Average horizontal displacement values of pile tops for different excavation depths.

Excavation Step	Excavation Depth (m)	Displacement of Pile Top (mm)
1	1.5	1.1
2	2.5	4.1
3	3.5	14.2
4	4.5	38.7

### 3.2. Earth Pressure Acting on the Pile

Figure 7 presents the variation of active and passive earth pressures acting on the piles with excavation depths of 1.5 m, 2.5 m, and 3.5 m, respectively. It can be observed that the active earth pressures all lie between the static earth pressure and the ultimate active earth pressure calculated by the Coulomb equation. A similar law can also be found in passive earth pressure. Moreover, the passive earth pressure is far less than the ultimate passive earth pressure calculated by the Coulomb equation. The reason is that the displacement of piles is too small to achieve passive ultimate soil displacement. Thus, the traditional calculation method of earth pressure needs to be modified before it can be applied to the design of retaining structures. As the excavation depth increases, the passive earth pressure increases gradually due to the increase in pile displacement. Furthermore, the active earth pressure becomes smaller and gradually approaches the ultimate active pressure calculated by the Coulomb equation, which means that the displacement of piles gradually approaches the active ultimate soil displacement. This highlights the significance of modifying the earth pressures acting on the pile based on the pile displacement.

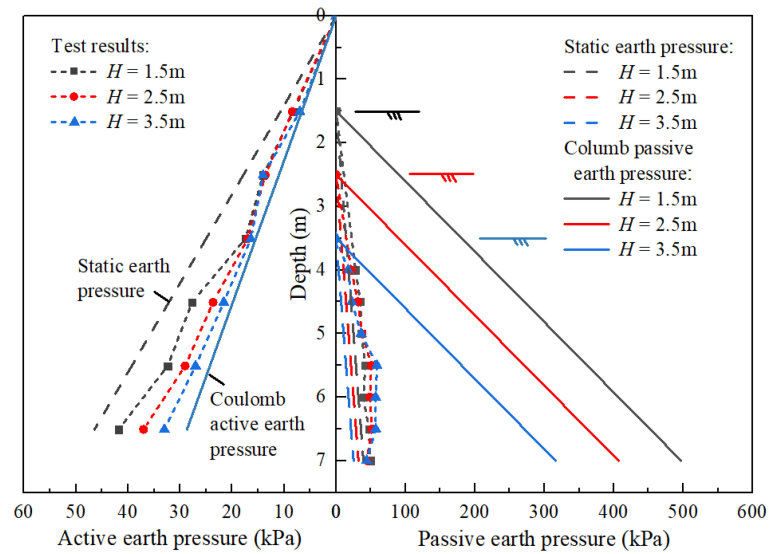


Figure 7. The active and passive earth pressure acting on the piles.

#### 4. Analytical Solution

Based on the aforementioned test phenomena and results, the following analytical solution for displacement-dependent earth pressure acting on the piles and the design method of ECR piles are proposed.

##### 4.1. Analytical Solutions for the Earth Pressures Acting on the Retaining Wall

Owing to the excavation of the soil in front of an embedded cantilevered retaining wall, movement of the wall consists generally of an approximately rigid rotation around a point located in proximity to the base of the structure [1,34,35]. Thus, to obtain the minimum critical length of piles, the assumed movement scheme of an ECR wall (pile) is shown in Figure 8.

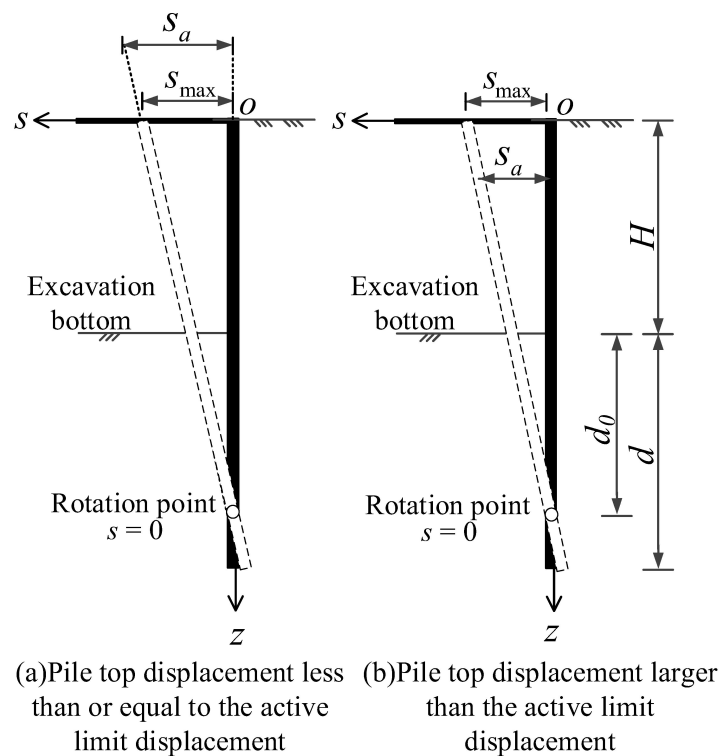
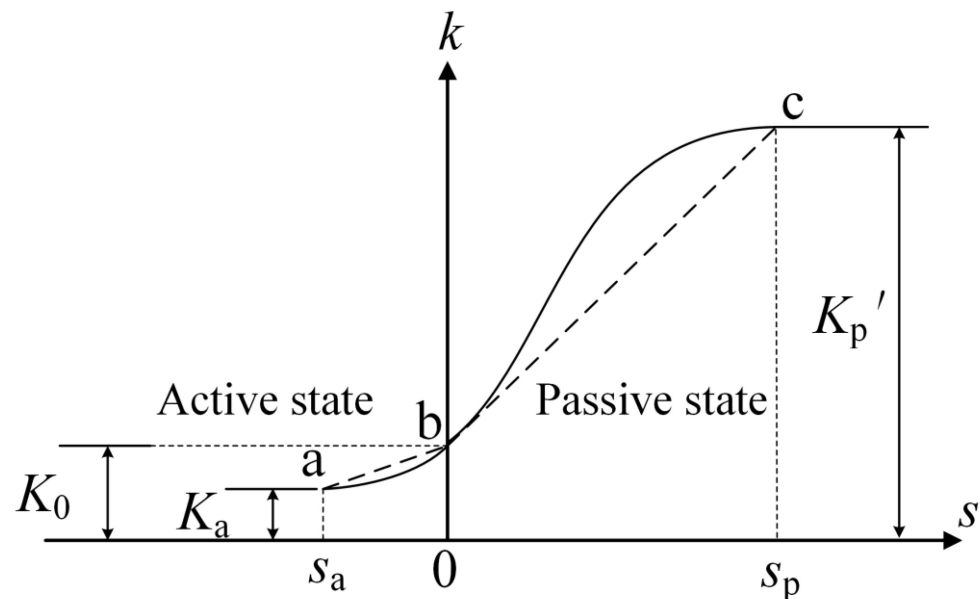


Figure 8. The assumed movement of ECR wall (pile).

Following this movement, a relationship between the earth pressure coefficient and the displacement can be established. For displacement  $s = 0$ , the earth pressure coefficient  $k = K_0$ , where  $K_0$  is the coefficient of earth pressure at rest and can be calculated using Jaky's equation [36]. After that, when the displacement  $s$  reaches the ultimate active passive state, the earth pressure coefficient  $k$  will reach  $K_a$  and  $K_p'$ , respectively, where  $K_a$  is the active earth pressure coefficient from the classic earth pressure theories (e.g., Coulomb theory and general wedge theory; Terzaghi [37]) and  $K_p'$  is revised from Coulomb theory [5]. For the soil displacement between 0 and the ultimate state, a linear relationship between the displacement  $s$  and the earth pressure coefficient  $k$  is assumed, as shown in Figure 9.



**Figure 9.** The assumed relationship between earth pressure coefficient  $k$  and horizontal displacement  $s$ .

The active and passive earth pressures for the ECR wall (pile) under excavation corresponding to any soil displacement can be obtained as follows:

$$p_a = \begin{cases} \left( (K_a - K_0) \frac{s}{s_a} + K_0 \right) \gamma z, & s \leq s_a \\ K_a \gamma z, & s > s_a \end{cases}, \quad (4)$$

$$p_p = \left( (K_p' - K_0) \frac{s}{s_p} + K_0 \right) \gamma (z - h), \quad (5)$$

where  $z$  represents the soil depth,  $K_a$  and  $K_p'$  [5] are the Coulomb active ultimate earth pressure and the revised Coulomb passive ultimate earth pressure [5], respectively, as follows:

$$K_a = \frac{\cos^2 \varphi}{(\cos \delta + \sqrt{\sin(\delta + \varphi) \cos \delta \sin \varphi})^2}, \quad (6)$$

$$K_p' = -2K_0 + 3K_p, \quad (7)$$

$$K_p = \frac{\cos^2 \varphi}{(\cos \delta - \sqrt{\sin(\delta + \varphi) \cos \delta \sin \varphi})^2} \quad (8)$$

In the formula,  $s_a$  and  $s_p$  refer to the required wall displacement to reach the ultimate active and passive earth pressure states. It has been proven that the  $s_a$  and  $s_p$  are related to the wall height,  $L$  and soil type. Studies by Clough and Duncan [38] have shown that the required wall displacement leading to the limit active state  $s_a$  is approximately  $0.001L$

to  $0.004L$  for sand, while  $s_a$  is approximately  $0.01L$  for clay. Likewise, it is also concluded that the required displacement resulting in the limit passive state  $s_p$  is approximately 10 times the  $s_a$ . Considering the strict displacement requirement of the retaining structure in engineering practice, the passive limit displacement is suggested to be set to a relatively small value, i.e.,  $(0.01\sim 0.05)d$ , or be tested by experiment.

4.2. Validation of the Analytical Solution of Earth Pressure

In order to evaluate the effectiveness and accuracy of the analytical solutions proposed above, the calculation results of the proposed solution for the earth pressure considering the soil displacement (i.e., Equations (4) and (5)) are compared with the foregoing model test results as well as the measured data and results in the existing literature [39,40]. The soil parameters of the tests in Fang et al. [39,40] are given in Table 2.

Table 2. Soil parameters of tests in Fang et al. [39,40].

Backfill	Soil State	$\gamma$ (kN/m <sup>3</sup> )	$\varphi$ (°)	$\delta$ (°)	$L$ (m)	References
Air-dry Ottawa sand	Active	15.4	34	16.7	1.015	[39]
	Passive	15.5	30.9	19.2	0.5	[40]

Figures 10–12 present the comparisons of the calculated and measured results of active and passive earth pressure by Fang et al. [39,40] and the proposed experiment, respectively. According to the test results in Fang et al. [39,40],  $s_a/L$  and  $s_p/L$  are 0.2‰ and 25% [5], respectively. It can be seen that, compared with Coulomb’s theoretical solution, the proposed displacement-based earth pressure modified method in this paper can reflect the nonlinear distribution of active and passive earth pressure as well as the magnitude of earth pressure more accurately. Therefore, the proposed solution has better applicability for the design of the ECR wall (pile).

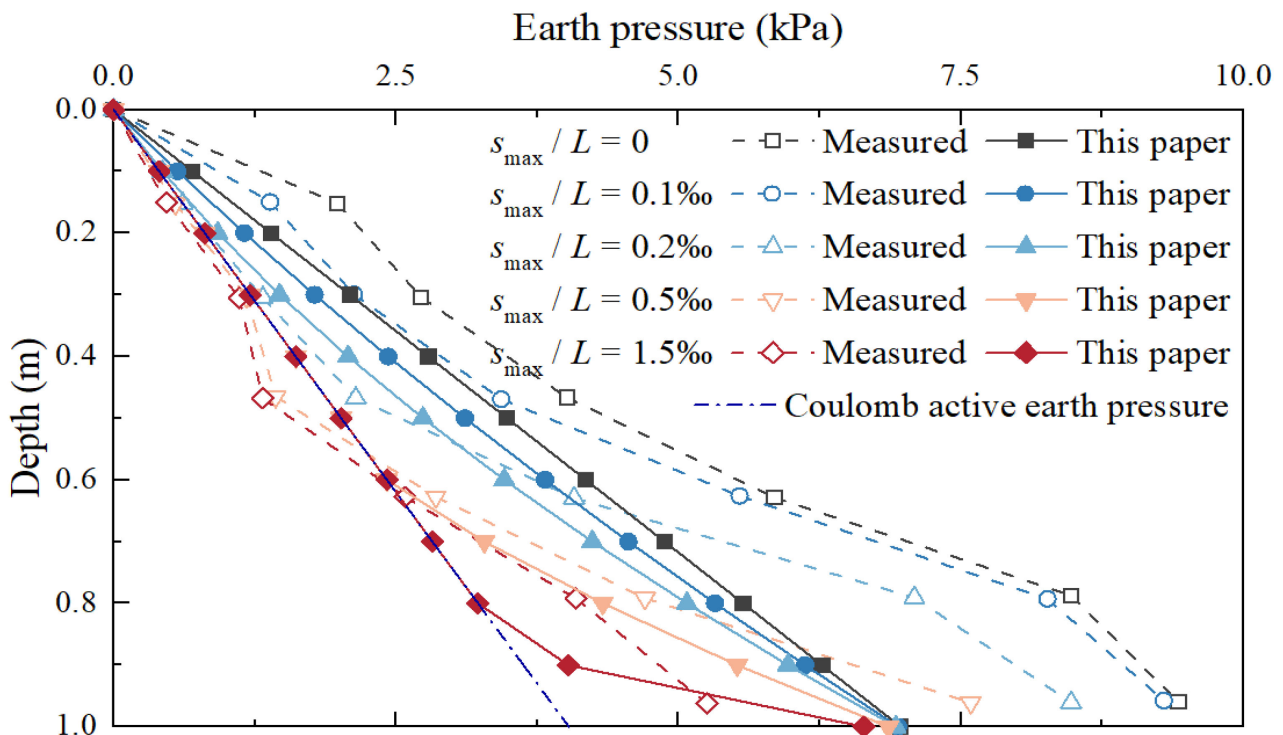


Figure 10. Comparison of active earth pressure between the analytical solution in this paper and test results in Fang et al. [39].

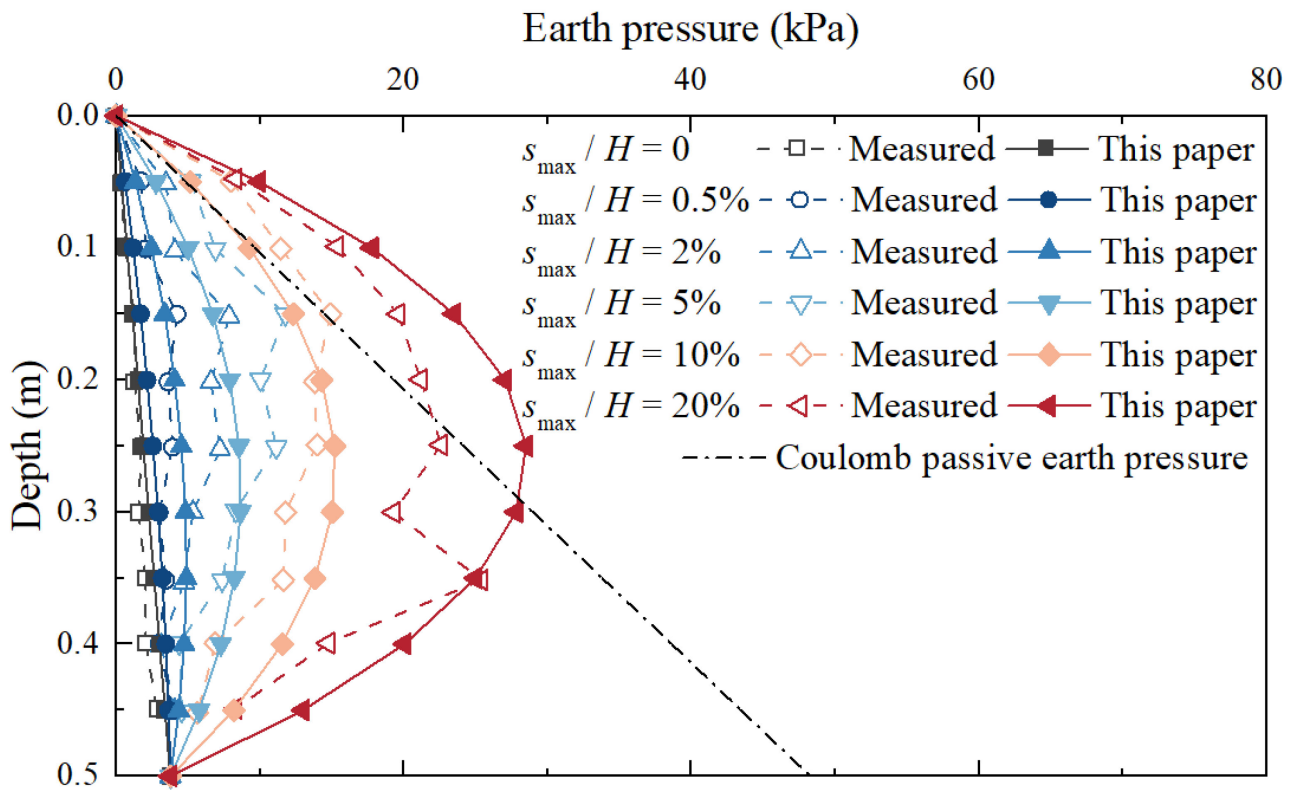


Figure 11. Comparison of passive earth pressure between the analytical solution in this paper and test results in Fang et al. [40]. (Reprinted with permission from Ref. [5]. 2021, Elsevier).

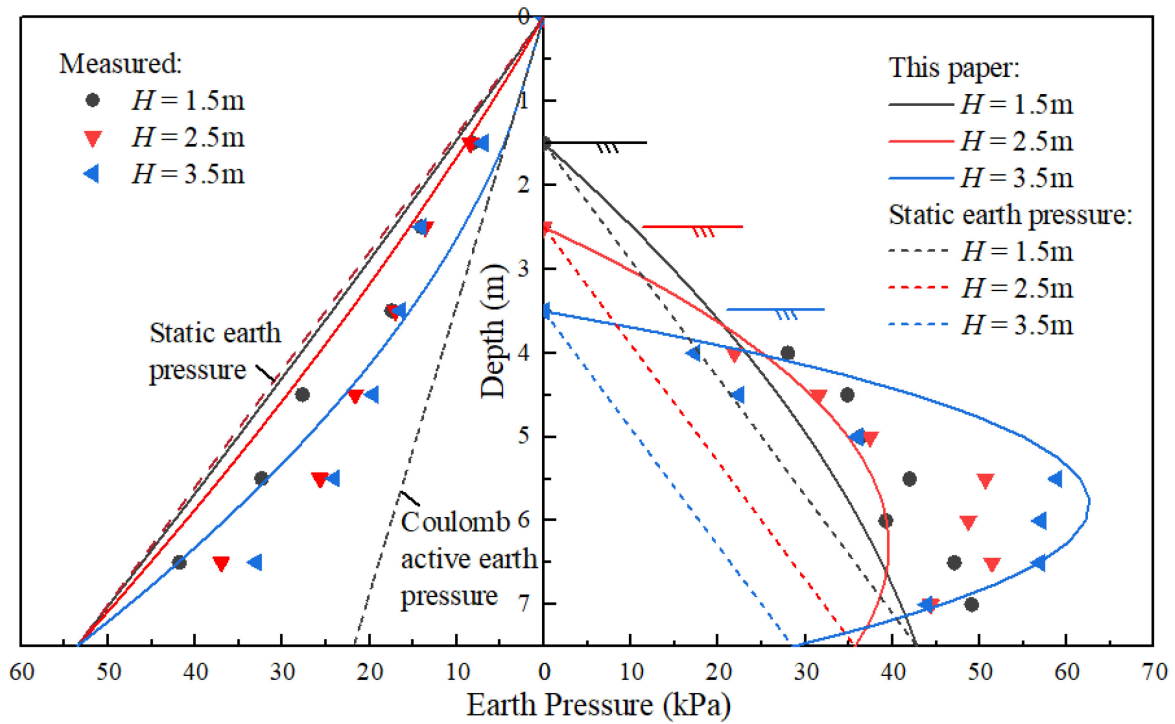


Figure 12. Comparison of earth pressure between the analytical solution and test results in this paper.

#### 4.3. Analytical Solution for the Deformation-Controlled Embedded Depth of Retaining Structure

According to the displacement movement model of the ECR wall (pile) in Figure 7a, the relationship between soil displacement  $s$  and the length of the supporting structure can be established as follows:

For the part above the rotation point:

$$s = \begin{cases} \frac{H+d_0-z}{H+d_0} s_{\max}, & s \leq s_a \\ s_a, & s > s_a \end{cases}, \quad (9)$$

For the part below the rotation point:

$$s = \begin{cases} \frac{z-H-d_0}{H+d_0} s_{\max}, & s \leq s_a \\ s_a, & s > s_a \end{cases}, \quad (10)$$

where  $s_{\max}$  is the limited maximum displacement of the pile top. In the design period,  $s_{\max}$  refers to the tolerated maximum displacement of the ECR wall (pile).

The earth pressure distribution assumed in the proposed method is shown in Figure 13. The earth pressure distribution above the rotation point consists of an active pressure  $p_{aarp}$  on the retained side and a passive pressure  $p_{parp}$  on the excavated side. Below the rotation point, soil goes from active to passive pressure, with a passive pressure  $p_{pbrp}$  on the retained side and an active pressure  $p_{abrp}$  on the excavated side.

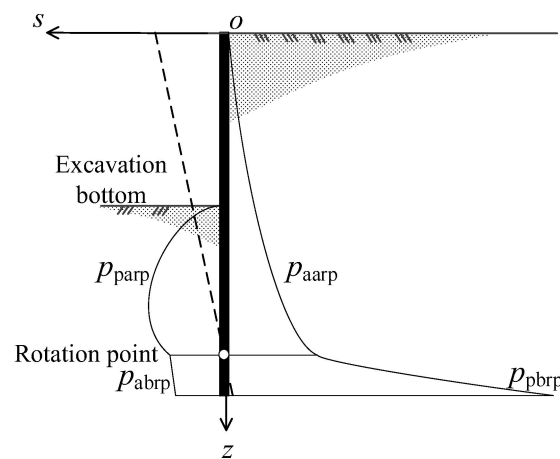


Figure 13. Distribution of earth pressures in the proposed method.

For the movement model as shown in Figure 8a, where  $s_{\max}$  does not exceed  $s_a$ , the distribution of lateral active earth pressure above the rotation point ( $p_{aarp}$ ) and below the rotation point ( $p_{abrp}$ ) can be obtained as follows:

$$p_{aarp} = (K_a - K_0) \frac{H + d_0 - z}{H + d_0} \frac{s_{\max}}{s_a} \gamma z + K_0 \gamma z, \quad (11)$$

$$p_{abrp} = (K_a - K_0) \frac{z - H - d_0}{H + d_0} \frac{s_{\max}}{s_a} \gamma (z - H) + K_0 \gamma (z - H), \quad (12)$$

As for the case in Figure 8b, where  $s_{\max}$  exceeds  $s_a$ , the distribution of lateral active earth pressure above the rotation point ( $p_{aarp}$ ) and below the rotation point ( $p_{abrp}$ ) should be replaced as follows:

$$p_{aarp} = \begin{cases} K_a \gamma z, & 0 \leq z \leq (H + d_0) \left(1 - \frac{s_a}{s_{\max}}\right) \\ (K_a - K_0) \frac{H + d_0 - z}{H + d_0} \frac{s_{\max}}{s_a} \gamma z + K_0 \gamma z, & (H + d_0) \left(1 - \frac{s_a}{s_{\max}}\right) < z \leq H + d_0 \end{cases}, \quad (13)$$

$$p_{abrp} = \begin{cases} K_a \gamma (z - H), & (H + d_0) \left(1 + \frac{s_a}{s_{\max}}\right) \leq z \leq H + d \\ (K_a - K_0) \frac{z - H - d_0}{H + d_0} \frac{s_{\max}}{s_a} \gamma (z - H) + K_0 \gamma (z - H), & H + d_0 \leq z < (H + d_0) \left(1 + \frac{s_a}{s_{\max}}\right) \end{cases} \quad (14)$$

In the same way, the formula for the passive earth pressure related to the displacement can be obtained as follows:

$$p_{parp} = (K'_p - K_0) \frac{H + d_0 - z}{H + d_0} \frac{s_{\max}}{s_p} \gamma (z - H) + K_0 \gamma (z - H), \quad (15)$$

$$p_{pbrp} = (K'_p - K_0) \frac{z - H - d_0}{H + d_0} \frac{s_{\max}}{s_p} \gamma z + K_0 \gamma z \quad (16)$$

The force equilibrium of the retaining structure can be established by considering the forces acting on the retained side ( $F_r$ ) and on the excavated side ( $F_e$ ) of the retaining structure:

$$F_r = \int_0^{H+d_0} (K_a - K_0) \frac{H + d_0 - z}{H + d_0} \frac{s_{\max}}{s_a} \gamma z dz + \int_0^{H+d} K_0 \gamma z dz + \int_{H+d_0}^{H+d} (K'_p - K_0) \frac{z - H - d_0}{H + d_0} \frac{s_{\max}}{s_p} \gamma z dz, \quad (17)$$

$$F_e = \int_H^{H+d_0} (K'_p - K_0) \frac{H + d_0 - z}{H + d_0} \frac{s_{\max}}{s_p} \gamma (z - H) dz + \int_H^{H+d} K_0 \gamma (z - H) dz + \int_{H+d_0}^{H+d} (K_a - K_0) \frac{z - H - d_0}{H + d_0} \frac{s_{\max}}{s_a} \gamma (z - H) dz \quad (18)$$

Similarly, the moment equilibrium can be established by taking the moment of the toe of the wall, generated by the forces acting on the retained side ( $M_r$ ) and on the excavated side ( $M_e$ ):

$$M_r = \int_0^{H+d_0} (K_a - K_0) \frac{H + d_0 - z}{H + d_0} \frac{s_{\max}}{s_a} \gamma z (H + d - z) dz + \int_0^{H+d} K_0 \gamma z (H + d - z) dz + \int_{H+d_0}^{H+d} (K'_p - K_0) \frac{z - H - d_0}{H + d_0} \frac{s_{\max}}{s_p} \gamma z (H + d - z) dz \quad (19)$$

$$M_e = \int_H^{H+d_0} (K'_p - K_0) \frac{H + d_0 - z}{H + d_0} \frac{s_{\max}}{s_p} \gamma (z - H) (H + d - z) dz + \int_H^{H+d} K_0 \gamma (z - H) (H + d - z) dz + \int_{H+d_0}^{H+d} (K_a - K_0) \frac{z - H - d_0}{H + d_0} \frac{s_{\max}}{s_a} \gamma (z - H) (H + d - z) dz \quad (20)$$

By equating  $F_r = F_e$  and  $M_r = M_e$ , a system of two equations for the two unknown parameters  $d_0$  and  $d$  is obtained. Additionally, if  $s_{\max}$  exceeds  $s_a$ , then the above Equations (17)–(20) should be piecewise integrals using Formulas (13) and (14).

#### 4.4. Parametric Analysis

In this section, a series of parametric studies are carried out to gain a greater understanding of the effects of the excavation depth and deformation control on the insertion ratio and the location of the rotation point. A typical type of cohesionless soil is applied for parametric analysis. For clays, the equivalent internal friction angle  $\varphi_e$  [41] according to the principle of equal shear strength can be introduced to represent incohesive soil. The equivalent equation is as follows:

$$\varphi_e = \arctan\left(\tan \varphi + \frac{c}{\gamma h}\right), \quad (21)$$

in which  $c$  is the cohesion of soil and  $h$  is the thickness of soil.

The soil parameters used in parametric analysis are given in Table 3.

**Table 3.** Soil parameters in parametric analysis.

$\Gamma$ (kN/m <sup>3</sup> )	$\varphi$ (°)	$\delta$ (°)	$s_a/L$ (%)	$s_p/L$ (%)
20	35	20	1	5

#### 4.4.1. Influence of the Excavation Depth

Figure 14a,b indicates the influence of excavation depth on the insertion ratio  $d/H$  and the location of the rotation point  $d_0/d$  under different controlled displacements  $s_{max}$ , respectively. It can be observed in Figure 14a that the required insertion ratio will increase as the excavation depth becomes deeper, and the increase rate will become larger with deeper excavation. Likewise, the controlled displacement shows a significant influence on the insertion ratio, which will be further discussed in Section 4.4.2.

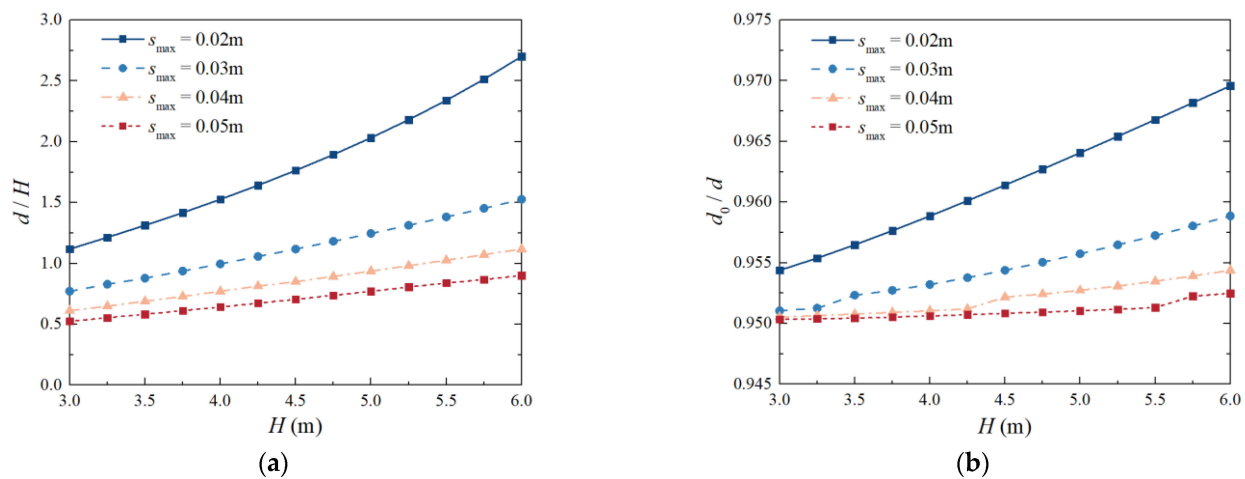


**Figure 14.** Influence of the excavation depth on the insertion ratio and the location of the rotation point: (a) Insertion ratio; (b) Location of the rotation point.

As shown in Figure 14b, as the  $s_{max}$  and the excavation depth  $H$  vary from 0.02 m to 0.05 m and 3.0 m to 6.0 m, respectively, the calculated values of  $d_0/d$  result in values between 0.95 and 0.97, indicating that the rotation point is located in proximity to the base of the ECR wall. This is consistent with the findings in the literature [1,34,35], which show the validity of the proposed solution. In addition, the location of the rotation point becomes closer to the wall base as the excavation depth increases. As well, sudden increases in the  $d_0/d$  can be observed in the curves of  $s_{max} = 0.03$  m, 0.04 m, and 0.05 m. The reason is that under those controlled displacements, the  $s_{max}$  will exceed  $s_a$  at some heights; therefore, those calculation results will be iterated using the piecewise integral as mentioned before.

#### 4.4.2. Influence of the Deformation Control

Figure 15a,b show the influence of the deformation control on the insertion ratio  $d/H$  and the location of the rotation point  $d_0/d$  under different excavation depths  $H$ , respectively. It can be observed from Figure 15a that, with the increase in the controlled displacement  $s_{max}$ , i.e., the reduction in deformation control requirements, the required insertion ratio gradually decreases. Likewise, as the deformation control becomes looser, the reduction rate of the required insertion ratio becomes slower. Moreover, under the same variation of the deformation control requirement, the deeper excavation depth shows a quicker reduction rate.

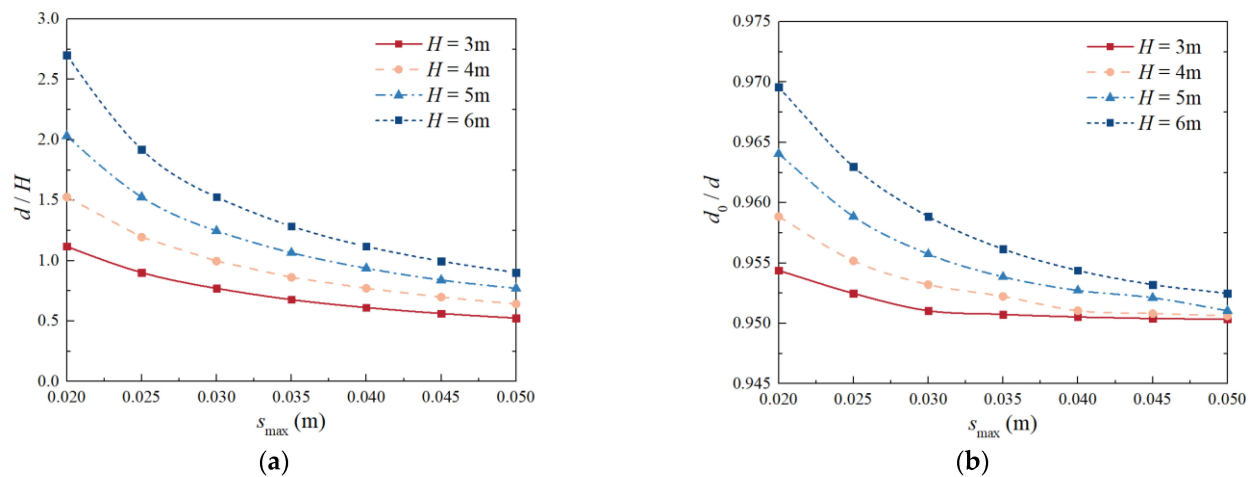


**Figure 15.** Influence of the controlled displacement on the insertion ratio and the location of the rotation point: (a) Insertion ratio; (b) Location of the rotation point.

As shown in Figure 15b, with the increase of the  $s_{\max}$ ,  $d_0/d$  gradually decreases, i.e., the position of the rotation point becomes relatively higher. However, the required insertion ratio will gradually decrease, and the deeper the foundation pit excavation is, the faster the reduction rate will be. Furthermore, sudden increases in the  $d_0/d$  can be observed in the curves of  $H = 4$  m, 5 m, and 6 m. The reason is that under those controlled displacements, in some cases the  $s_{\max}$  exceeds the  $s_a$ ; therefore, those calculation results will be iterated using the piecewise integral as mentioned before.

## 5. Conclusions

Displacement control is critical to the design of retaining walls in order to avoid any potential damage to adjacent structures and improve the sustainability of the surrounding environment. Current design practice for ECR walls (piles) is generally based on the limit equilibrium method, which cannot reasonably consider the displacement control of ECR walls (piles). Although research regarding the deformation control design of ECR walls (piles) has been carried out, a realistic and simple-to-use design method that can calculate the required embedment depth based on the deformation control is still to be explored. Based on an assumed linear relationship between the earth pressure coefficient and soil displacement, this paper proposes a deformation-controlled design method for the calculation of the required embedment depth.

In this paper, model tests are first conducted to investigate the deformation and earth pressure distribution of the ECR wall during excavations. Based on the experimental observations, a displacement-dependent non-limited earth pressure coefficient is proposed to derive an analytical solution to predict both the active and passive earth pressure acting on the ECR wall. The proposed solution is validated by comparing the proposed results with the existing and presented experiment results. On the basis of the proposed solution for earth pressure, a displacement-controlled method for calculating the embedment depth and the location of the rotation point of ECR is proposed. Parametric studies are conducted to demonstrate the impact of deformation control and excavation depth on the design parameters of retaining walls. Then, the following conclusions are drawn:

(1) The required insertion ratio will increase with the growth of excavation depth and the enhancement of deformation control requirements. Likewise, the increase rate will become larger with deeper excavation and stricter deformation control requirements.

(2) The rotation point is located in proximity to the base of the ECR wall. Furthermore, the location is closer to the wall base with the growth of excavation depth and the enhancement of deformation control requirements.

**Author Contributions:** Conceptualization, X.F. and C.X.; methodology, X.F.; validation, X.F.; formal analysis, X.F.; investigation, X.F. and L.L.; writing—original draft preparation, X.F.; writing—review and editing, X.F., C.X. and L.L.; funding acquisition, X.F., C.X. and L.L. All authors have read and agreed to the published version of the manuscript.

**Funding:** This research was funded by the National Natural Science Foundation of China, grant number 52238009; the Zhejiang Provincial Natural Science Foundation of China, grant numbers LQ23E080002 and LQ22E080009; and the National Science Fund of Jiangxi Province, grant number 20223BBG71018.

**Data Availability Statement:** The data presented in this study are available on request from the corresponding author.

**Conflicts of Interest:** The authors declare no conflict of interest.

## Abbreviations

$G_s$	specific gravity of soil;
$D_{10}/D_{30}/D_{60}$	Effective/average/limited particle size on the particle accumulation curve;
$\gamma$	dry unit weight of soil;
$e$	void ratio of soil;
$\varphi$	internal friction angle of soil;
$\delta$	external friction angle of soil;
$c$	cohesion of soil;
$h$	soil thickness;
$s$	horizontal displacement of wall (pile) (m);
$z$	pile/soil depth (m);
$k_s$	horizontal resistance coefficient (N/m <sup>3</sup> );
$b_0$	calculated width of wall (pile) (m);
$EI$	pile bending stiffness (N·m <sup>2</sup> );
$\lambda_L/\lambda_E$	length/elasticity modulus scale;
$\lambda_{k_s}$	horizontal resistance coefficient scale;
$d_{50}$	characteristic particle size (m);
$B$	diameter of pile (m);
$H$	excavation depth (m);
$d_0$	depth from pit bottom to the rotation point;
$d$	insertion depth of retaining wall (pile);
$k$	earth pressure coefficient;
$K_0$	at rest earth pressure coefficient;
$K_a/K_p$	active/passive earth pressure coefficient;
$K_p'$	modified passive earth pressure coefficient;
$p_a/p_p$	active/passive earth pressure;
$L$	retaining wall (pile) length;
$p_{aarp}/p_{abrp}$	active earth pressure above/below the rotation point;
$p_{parp}/p_{pbrp}$	passive earth pressure above/below the rotation point;
$F_r/F_e$	force acting on the retained/excavated side;
$M_r/M_e$	forces acting on the retained/excavated side;

## References

1. Conte, E.; Troncone, A.; Vena, M. A method for the design of embedded cantilever retaining walls under static and seismic loading. *Géotechnique* **2017**, *67*, 1081–1089. [[CrossRef](#)]
2. Boscardin, M.D.; Cording, E.J. Building response to excavation-induced settlement. *J. Geotech. Eng.* **1989**, *115*, 1–21. [[CrossRef](#)]
3. Finno, R.J.; Voss, F.T., Jr.; Rossow, E.; Blackburn, J.T. Evaluating damage potential in buildings affected by excavations. *J. Geotech. Geoenviron. Eng.* **2005**, *131*, 1199–1210. [[CrossRef](#)]
4. Schuster, M.; Kung, G.T.C.; Juang, C.H.; Hashash, Y.M. Simplified model for evaluating damage potential of buildings adjacent to a braced excavation. *J. Geotech. Geoenviron. Eng.* **2009**, *135*, 1823–1835. [[CrossRef](#)]
5. Fan, X.Z.; Xu, C.J.; Liang, L.J.; Chen, Q.Z.; Deng, J.L. Analytical solution for displacement-dependent passive earth pressure on rigid walls with various wall movements in cohesionless soil. *Comput. Geotech.* **2021**, *140*, 104470. [[CrossRef](#)]

6. Fan, X.Z.; Phoon, K.K.; Xu, C.J.; Tang, C. Closed-form solution for excavation-induced ground settlement profile in clay. *Comput. Geotech.* **2021**, *137*, 104266. [[CrossRef](#)]
7. Son, M.; Cording, E.J. Estimation of building damage due to excavation-induced ground movements. *J. Geotech. Geoenviron. Eng.* **2005**, *131*, 162–177. [[CrossRef](#)]
8. Son, M.; Cording, E.J. Responses of buildings with different structural types to excavation-induced ground settlements. *J. Geotech. Geoenviron. Eng.* **2011**, *137*, 323–333. [[CrossRef](#)]
9. Wang, L.; Luo, Z.; Xiao, J.; Juang, C.H. Probabilistic inverse analysis of excavation-induced wall and ground responses for assessing damage potential of adjacent buildings. *Geotech. Geol. Eng.* **2014**, *32*, 273–285. [[CrossRef](#)]
10. Dalgic, K.D.; Hendriks, M.A.; Ilki, A. Building response to tunnelling-and excavation-induced ground movements: Using transfer functions to review the limiting tensile strain method. *Struct. Infrastruct. Eng.* **2018**, *14*, 766–779. [[CrossRef](#)]
11. Hsiao, E.C.; Schuster, M.; Juang, C.H.; Kung, G.T. Reliability analysis and updating of excavation-induced ground settlement for building serviceability assessment. *J. Geotech. Geoenviron. Eng.* **2008**, *134*, 1448–1458. [[CrossRef](#)]
12. Juang, C.H.; Schuster, M.; Ou, C.Y.; Phoon, K.K. Fully probabilistic framework for evaluating excavation-induced damage potential of adjacent buildings. *J. Geotech. Geoenviron. Eng.* **2011**, *137*, 130–139. [[CrossRef](#)]
13. Zhang, J.Z.; Phoon, K.K.; Zhang, D.M.; Huang, H.W.; Tang, C. Novel approach to estimate vertical scale of fluctuation based on CPT data using convolutional neural networks. *Eng. Geol.* **2021**, *294*, 106342. [[CrossRef](#)]
14. Li, Q.; Chen, G.; Luo, D.; Ma, H.; Liu, Y. An experimental study of a novel liquid carbon dioxide rock-breaking technology. *Int. J. Rock Mech. Min.* **2020**, *128*, 104244. [[CrossRef](#)]
15. Zhang, J.Z.; Huang, H.W.; Zhang, D.M.; Phoon, K.K. Experimental study of the coupling effect on segmental shield tunnel lining under surcharge loading and excavation unloading. *Tunn. Undergr. Sp. Tech.* **2023**, *140*, 105199. [[CrossRef](#)]
16. Chen, G.; Li, Q.; Li, D.; Wu, Z.; Liu, Y. Main frequency band of blast vibration signal based on wavelet packet transform. *Appl. Math. Model.* **2019**, *74*, 569–585. [[CrossRef](#)]
17. Ou, C.Y.; Liao, J.T.; Cheng, W.L. Building response and ground movements induced by a deep excavation. *Géotechnique* **2000**, *50*, 209–220. [[CrossRef](#)]
18. Wang, J.H.; Xu, Z.H.; Wang, W.D. Wall and ground movements due to deep excavations in Shanghai soft soils. *J. Geotech. Geoenviron. Eng.* **2010**, *7*, 136. [[CrossRef](#)]
19. Zhang, D.M.; Phoon, K.K.; Huang, H.W.; Hu, Q.F. Characterization of Model Uncertainty for Cantilever Deflections in Undrained Clay. *J. Geotech. Geoenviron. Eng.* **2015**, *141*, 04014088. [[CrossRef](#)]
20. Nandi, R.; Choudhury, D. Displacement-controlled approach for the analysis of embedded cantilever retaining walls with a distanced strip surcharge. *Comput. Geotech.* **2022**, *151*, 104970. [[CrossRef](#)]
21. Nandi, R.; Choudhury, D. Displacement-controlled analysis of embedded cantilever retaining walls. *Int. J. Geomech.* **2023**, *23*, 06023005. [[CrossRef](#)]
22. King, G.J.W. Analysis of cantilever sheet-pile walls in cohesionless soil. *J. Geotech. Eng.* **1995**, *121*, 629–635. [[CrossRef](#)]
23. Powrie, W. Limit equilibrium analysis of embedded retaining walls. *Géotechnique* **1996**, *46*, 709–723. [[CrossRef](#)]
24. Day, R.A. Net pressure analysis of cantilever sheet pilewalls. *Géotechnique* **1999**, *49*, 231–245. [[CrossRef](#)]
25. Madabhushi, S.P.G.; Chandrasekaran, V.S. Rotation of cantilever sheet pile walls. *J. Geotech. Geoenviron. Eng.* **2005**, *131*, 202–212. [[CrossRef](#)]
26. Gajan, S. Normalized relationships for depth of embedment of sheet pile walls and soldier pile walls in cohesionless soils. *Soils Found.* **2011**, *51*, 559–564. [[CrossRef](#)]
27. Conte, E.; Troncone, A. Simplified analysis of cantilever diaphragm walls in cohesive soils. *Soils Found.* **2018**, *58*, 1446–1457. [[CrossRef](#)]
28. Zhou, J.; Qin, C. Limit state analysis of rigid retaining structures against seismically induced passive failure in heterogeneous soils. *J. Rock Mech. Geotech.* **2023**, *in press*. [[CrossRef](#)]
29. Burland, J.B.; Potts, D.M.; Walsh, N.M. The overall stability of free and propped embedded cantilever retaining walls. *Ground. Eng.* **1981**, *14*, 28–37.
30. Valsangkar, A.J.; Schriver, A.B. Partial and total factors of safety in anchored sheet pile design. *Can. Geotech. J.* **1991**, *28*, 812–817. [[CrossRef](#)]
31. *D2487-11*; Standard Practice for Classification of Soils for Engineering Purpose. ASTM: West Conshohocken, PA, USA, 2011.
32. Lin, H.; Lei, G.; Xu, L.; Lei, G. Similarity analysis of deflection behavior of laterally loaded piles in 1g model tests. *J. Central South Uni. (Sci. Tech.)* **2012**, *43*, 3639–3645. (In Chinese)
33. Fioravante, V. On the shaft friction modelling of non-displacement piles in sand. *Soils Found.* **2002**, *42*, 23–33. [[CrossRef](#)]
34. Bolton, M.D.; Powrie, W. Collapse of diaphragm walls retaining clay. *Géotechnique* **1987**, *37*, 335–353. [[CrossRef](#)]
35. Clough, G.W.G.; O'Rourke, T.T.D. Construction induced movements of in situ walls. In *Proceedings Design and Performance of Earth Retaining Structures*; ASCE: New York, NY, USA, 1990; pp. 439–470.
36. Jaky, J. Pressure in soils. In *Proceedings of the 2nd International Conference on Soil Mechanics and Foundation Engineering*, Rotterdam, The Netherlands, 21–30 June 1948; pp. 103–107.
37. Terzaghi, K. *Theoretical Soil Mechanics*; Wiley: New York, NY, USA, 1943.
38. Clough, G.W.; Duncan, J.M. Earth Pressures. In *Foundation Engineering Handbook*; Springer: Boston, MA, USA, 1991; pp. 223–235.
39. Fang, Y.S.; Ishibashi, I. Static earth pressures with various wall movements. *J. Geotech. Eng.* **1986**, *112*, 317–333. [[CrossRef](#)]

40. Fang, Y.S.; Chen, T.; Wu, B. Passive earth pressures with various wall movements. *J. Geotech. Eng.* **1994**, *120*, 1307–1323. [[CrossRef](#)]
41. Liu, G.; Wang, W. *Excavation Engineering Manual*; China Architecture and Building Press: Beijing, China, 2009; pp. 105–145. (In Chinese)

**Disclaimer/Publisher's Note:** The statements, opinions and data contained in all publications are solely those of the individual author(s) and contributor(s) and not of MDPI and/or the editor(s). MDPI and/or the editor(s) disclaim responsibility for any injury to people or property resulting from any ideas, methods, instructions or products referred to in the content.